ACS APPLIED MATERIALS & INTERFACES

Research Article

www.acsami.org

Effects of Alkyl Chain Length on the Optoelectronic Properties and Performance of Pyrrolo-Perylene Solar Cells

Xianqing Liu,[†,∥] Yu Jin Kim,[‡,∥] Yeon Hee Ha,[†] Qinghua Zhao,[§] Chan Eon Park,*[,‡] and Yun-Hi Kim*[,†]

[†]Department of Chemistry and Research Institute of for Green Energy Convergence Technology (RIGET), Gyeongsang National University, Jinju, 660-701, Republic of Korea

[‡]POSTECH Organic Electronics Laboratory, Department of Chemical Engineering, Pohang University of Science and Technology, Pohang, 790-784, Republic of Korea

[§]Department of Polymer Science and Engineering, Huaqiao University, Quanzhou, China

ABSTRACT: While the impact of alkyl side-chain length on the photovoltaic properties of conjugated polymers and their performance in bulk heterojunction (BHJ) solar cells has been studied extensively, analogous studies on pyrrolo-perylene-based polymers have not received adequate attention. To explore these effects, we synthesized two copolymers based on *N*-annulated pyrrolo-perylene and consisting of cyano group substituents on thiophene vinylene thiophene units with two different alkyl groups of 2-decyltetradecyl and 7-decylnonadecyl, and we studied them with regard to chemical structure and photovoltaic performance. UV−vis spectroscopy and cyclic voltammetry studies showed that variations in alkyl chain length affect crystallization, light absorption, and the highest occupied molecular orbital and lowest unoccupied molecular orbital energy levels. These factors have a pronounced impact on the morphology of BHJ thin films and their charge carrier separation and transportation characteristics, which, in turn, influences photovoltaic properties.

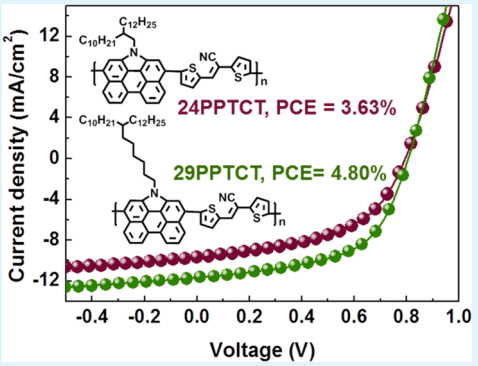

KEYWORDS: *organic solar cell, bulk heterojunction solar cell, conjugated polymer, alkyl side chain, pyrrolo-perylene unit*

INTRODUCTION

Bulk heterojunction (BHJ) organic solar cells (OSCs) have attracted considerable attention as sunlight harvesting devices because they can be fabricated at low cost on flexible substrates using roll-to-roll coating technologies.[1−3] To date, BHJ OSCs composed of low-bandgap polymers and [6,6]-phenyl-C_{71}-butyric acid methyl ester ($PC_{71}BM$) have exhibited power conversion efficiencies (PCEs) exceeding 9% in a single junction solar cell.[4,5] Intensive efforts are underway aimed at developing even more efficient BHJ OSCs through the design and synthesis of new polymeric donor materials.[6,7] Among the strategies being explored, side-chain engineering has shown considerable potential for the development of high-performance photovoltaic polymers.[8−12] Indeed, the crystallinity of such polymers in the solid state, and their solubility in organic solvents are directly controlled by the characteristics of the alkyl side chains of the polymer backbone. Proper selection of the tethering position, length, and bulkiness of these side chains is paramount for obtaining desired photovoltaic properties.[13−16]

The present work focuses on the effects of alkyl chain length in push−pull conjugated polymers. Thiophene vinylene thiophene, with cyano groups as electron-withdrawing units[17,18] and *N*-annulated pyrrolo-perylene units as electron-donating units, were selected due to their structural symmetry and rigid fused aromatic system. These characteristics promote electron delocalization and molecular packing.[19,20] There have been surprisingly few investigations of the effects of alkyl side chain geometry in pyrrolo-perylene polymers.

We report herein a systematic study of two high-efficiency, low band gap pyrrolo-perylene polymers, 24PPTCT and 29PPTCT, with different alkyl side chains. The replacement of a 2-decyltetradecyl side chain with a longer 7-decylnonadecyl side chain resulted in significant changes in the crystallization characteristics, optoelectronic properties, and morphological structure of the polymers. These changes, in turn, had a significant impact on the subsequent photovoltaic performance of OSCs based on these polymers. To determine the mechanism(s) underlying these effects, we analyzed OSC devices made with 24PPTCT and 29PPTCT spectroscopically and determined structure-performance relationships. Significant differences in the photovoltaic performance of the two polymer blends emanate from the different side chain lengths, which affect morphology and charge transport. This finding provides valuable insight for the development of efficient pyrrolo-perylene OSCs.

EXPERIMENTAL SECTION

Materials. Pd_2 $(dba)_3$ and $P(o\text{-Tol})_3$ were purchased from Umicore. All reactions were performed using standard Schlenk

Received: February 16, 2015
Accepted: April 3, 2015
Published: April 3, 2015

DOI: 10.1021/acsami.5b01444
ACS Appl. Mater. Interfaces 2015, 7, 8859−8867

techniques under a nitrogen atmosphere. All chemical reagents were purchased from Aldrich and used as received.

Synthesis of Monomers and Polymers. *1-Nitroperylene (1).* Compound **1** was synthesized according to the literature.[21] ^{1}H NMR (DMSO, 300 MHz): 8.53−8.57 (d, 2H), 7.95−8.04 (m, 4H), 7.68−7.85 (m, 4H), 7.57−7.60(t, 1H).

1H-Phenanthro[1,10,9,8-cdefg]carbazole (2). Compound **2** was also synthesized according to the literature.[21] ^{1}H NMR (DMSO 300 MHz): 12.21 (s, 1H), 8.74−8.77 (d, 2H), 8.17−8.19 (d, 2H), 7.92−7.99 (t, 4H), 7.79−7.85 (t, 2H).

1-(2-Decyltetradecyl)-1H-phenanthro[1,10,9,8-cdefg]carbazole (3). Compound **3** was also synthesized according to the literature.[21] ^{1}H NMR ($CDCl_3$, 300 MHz): d (ppm) 8.60−8.63 (d, 2H), 8.10−8.14 (d, 2H), 7.91−7.93 (d, 2H), 7.84−7.85 (d, 2H), 7.84−7.91 (t, 2H), 4.28−4.32 (d, 2H), 2.16 (m, 1H), 1.10−1.42 (m, 40H), 0.85−0.91 (m, 6H).

1-(7-Decylnonadecyl)-1H-phenanthro[1,10,9,8-cdefg]carbazole (4). Under nitrogen atmosphere, compound **2** (4 g, 14.4 mmol), NaH (0.60 g, 25.2 mmol), 11-(6-bromohexyl)tricosane (12.0 g, 22.8 mmol) was dissolved into dry THF and then stirred at 66 °C for 12 h. The reaction mixture was then cooled to room temperature, poured into water and extracted with dichloromethane. The organic solution was dried with plenty of anhydrous magnesium sulfate and evaporation under low pressure. The crude product was purified by column chromatography on silica gel with *n*-hexane as eluent and yielded a product like yellow oil. (Yield: 6.5 g, 65.3%) ^{1}H NMR ($CDCl_3$, 300 MHz): d (ppm) 8.66−8.68 (d, 2H), 8.13−8.16 (d, 2H), 7.92−7.95 (d, 2H), 7.84−7.85 (d, 2H), 7.85−7.91 (t, 2H), 4.71−4.75 (t, 2H), 2.12 (m, 1H), 1.10−1.42 (m, 49H), 0.85−0.91 (m, 6H).

3,10-Dibromo-1-(2-decyltetradecyl)-1H-phenanthro[1,10,9,8-cdefg]carbazole (M_1). With the absent of light, compound 3 (6.5 g, 10.8 mmol) was dissolved into dichloromethane. NBS (3.84 g, 21.6 mmol) was added into the solution, and the resulting mixture was stirred at room temperature for 6 h. Then, the reaction mixture was poured into water and extracted with dichloromethane. The organic solution was dried with plenty of anhydrous magnesium sulfate and evaporation under low pressure. The crude product was purified by column chromatography on silica gel with *n*-hexane as eluent and yielded a yellow product. (Yield: 4.93 g, 59.7%) ^{1}H NMR ($CDCl_3$, 300 MHz): d (ppm) 8.60−8.63 (d, 2H), 8.29−8.32 (d, 2H), 7.94 (s, 2H), 7.85−7.91 (t, 2H), 4.29−4.32 (d, 2H), 2.14 (m, 1H), 1.10−1.42 (m, 40H), 0.85−0.91 (m, 6H). MS (EI) *m*/*z*: 759 (M^+).

3,10-Dibromo-1-(7-decylnonadecyl)-1H-phenanthro[1,10,9,8-cdefg]carbazole (M_2). With the absent of light, compound **4** (6.5 g, 9.68 mmol) was dissolved into dichloromethane. NBS (3.45 g, 19.4 mmol) was added into the solution, and then the reaction mixture was stirred at room temperature for 6 h. The reaction mixture was poured into water and extracted with dichloromethane. The organic solution was dried with plenty of anhydrous magnesium sulfate and evaporation under low pressure. The crude product was purified by column chromatography on silica gel with *n*-hexane as eluent and yielded a yellow product. (Yield: 5.6 g, 67.3%) ^{1}H NMR ($CDCl_3$, 300 MHz): d (ppm) 8.69−8.72 (d, 2 H), 8.36−8.39 (d, 2 H), 8.11 (s, 2 H), 7.90−7.93 (t, 2 H), 4.60−4.64 (t, 2 H), 2.06−2.12 (m, 1 H), 1.18−1.37 (m, 49 H), 0.87−0.91 (m, 6 H). MS (EI) *m*/*z*: 829 (M+).

(E)-2,3-Bis(5-(trimethylstannyl)thiophen-2-yl)acrylonitrile (M). Monomer M was synthesized referring to the literature.[22] ^{1}H NMR (300 MHz, $CDCl_3$) d (ppm): δ 7.66−7.65 (d, 1H), 7.56 (s, 1H), 7.43−7.42 (d, 1H), 7.22−7.21 (d, 1H), 7.15−7.13 (d, 1H), 0.53−0.32 (m, 18H).

Polymerization of 24PPTCT. In a 25 mL dry flask, monomer M_1 (0.3 g, 0.394 mmol) and monomer M (0.214g, 0.394 mmol) were dissolved in 12 mL of chlorobenzene, and the mixture was subjected to bubbling with nitrogen for 30 min. Pd_2 $(dba)_3$ (7.2 mg, 0.00790 mmol) and P(*o*-Tol)$_3$ (9.6 mg, 0.0316 mmol) were added, and the resulting mixture was stirred for 48 h at 110 °C afterward. Subsequently, for end-capping, 2-bromothiophene and tributyl-(thiophen-2-yl)stannane were added into the flask, and the reaction mixture was stirred for 6 h. The resulting mixture was then dropped into methanol (300 mL with 5 mL of HCl aq), causing the polymer to precipitate as pellets. The crude polymer was collected by filtration and purified by Soxhlet extraction with methanol, acetone, hexane, toluene, chloroform, 1-bromobenzene and 1,2-dibromobenzene, successively. The 24PPTCT was obtained by precipitation of the chloroform solution into methanol. (Yield: 0.082 g, 22.4%, M_n = 21 200 g/mol, M_w = 30 104 g/mol, PDI = 1.42) ^{1}H NMR (500 MHz, $CDCl_3$) d (ppm): δ 8.43 (br, 4H), 7.84 (br, 4H), 7.60 (br, 2H), 7.44 (br, 2H), 4.44−4.62 (br, 2H), 2.1 (s, 1H), 1.1 (br, 40), 0.77 (br, 6).

Polymerization of 29PPTCT. In a 25 mL dry flask, monomer M_2 (0.3 g, 0.362 mmol) and monomer M (0.196 g, 0.362 mmol) was dissolved in 12 mL of chlorobenzene, then bubbling with nitrogen for 30 min. Pd_2 $(dba)_3$ (6.6 mg, 0.0072 mmol) and P(*o*-Tol)$_3$ (8.8 mg, 0.0289) were added, and the resulting mixture was stirred for 48 h at 110 °C. Then, for end-capping, 2-bromothiophene and tributyl-(thiophen-2-yl)stannane were added into the flask and the reaction mixture was stirred for 6 h. The reaction mixture was then dropped into methanol (300 mL with 5 mL HCl aq), causing the polymer to precipitate as pellets. The crude polymer was collected by filtration and purified by Soxhlet extraction with methanol, acetone, hexane, toluene, chloroform, 1-bromobenzene and 1,2-dibromobenzene, successively. The 29PPTCT was obtained by precipitation of the chloroform solution into methanol. (Yield: 0.21 g, 65.6%, M_n = 23 400 g/mol, M_w = 30 654 g/mol, PDI = 1.31) ^{1}H NMR (500 MHz, $CDCl_3$) d (ppm): δ 8.28−8.41 (br, 4H), 7.87 (br, 4H), 7.60 (br, 2H), 7.40 (br, 2H), 4.06−4.62 (br, 2H), 2.1 (s, 1H), 1.12−1.18 (br, 49), 0.77 (br, 6).

General Measurements. ^{1}H NMR and ^{13}C NMR spectra were recorded using a Bruker Advance-300 spectrometer and DRX-500 MHz spectrometer. HRMS (EI) spectra were obtained using a high-resolution gas chromatography (GC) mass spectrometer with a LabRAM HR800 UV. Mass spectra were recorded using a high-resolution 4800 TOF/TOF mass spectrometer with Voyager DE-STR. Copolymer molecular weights and polydispersities were determined by gel-permeation chromatography (GPC) using a polystyrene standard. In the GPC, water was used as the mobile phase in a high-pressure GPC assembly using a Model M515 pump with u-Styragel columns of HR4, HR4E, and HR5E, which yielded 500 and 100 Å resolutions. Thermogravimetric analysis (TGA) was performed on a TA TGA 2100 analyzer under purified nitrogen at a heating rate of 10 °C/min. Differential scanning calorimetry (DSC) was conducted under nitrogen on a TA Instruments 2100 DSC. Samples were heated to 10 °C/min from 50 to 250 °C. The UV−vis absorption spectra were recorded using a Cary 5000 UV−vis−near-IR double beam spectrophotometer. Cyclic voltammetry (CV) was performed using a PowerLab/AD instrument model system in a 0.1 M tetrabutylammonium hexafluorophosphate (Bu_4NPF_6) solution in anhydrous acetonitrile as the supporting electrolyte, at a scan rate of 50 mV/s. A glassy carbon disk (~0.05 cm^2) coated with a thin polymer film, an Ag/AgCl electrode and a platinum wire were used as the working, reference and counter electrodes, respectively. Atomic force microscopy (AFM) was conducted using a Multimode IIIa microscope (Digital Instruments) in tapping mode to obtain surface images (surface area: 5 × 5 μm) of the pure polymer and polymer:$PC_{71}BM$ blend films under ambient conditions.

Fabrication and Characterization of photovoltaic devices and hole-only devices. Photovoltaic devices with the structure ITO/PEDOT:PSS/polymer:$PC_{71}BM$/Al or Ca/Al were fabricated. The indium tin oxide (ITO)-coated glass substrate was cleaned by successive sonication in detergent, distilled water, acetone, and isopropyl alcohol. A 40 nm thick layer of PEDOT:PSS (Clevios P VP AI 4083, filtered at 0.45 μm PVDF) was spin-coated on the cleaned ITO substrate that had been exposed to ozone for 20 min. The PEDOT:PSS layer was baked on a hot plate at 120 °C for 15 min, and then the substrates were transferred into a nitrogen-filled glovebox. The active layer was then spin-coated onto the PEDOT:PSS layer from a predissolved composite solution that had been filtered through a 0.45 μm syringe filter. Finally, as the top electrode, an Al or Ca (5 nm)/Al cathode (100 nm) was deposited onto the active layer under vacuum (2 × 10^{-6} Torr) in a thermal evaporator. In the final solar cells, the active layer area was 0.09 cm^2. The current density−voltage (*J*−*V*) characteristics of the photovoltaic devices were measured under ambient conditions using a Keithley Model 2400

DOI: 10.1021/acsami.5b01444
ACS Appl. Mater. Interfaces 2015, 7, 8859−8867

Scheme 1. Synthetic Routes and Chemical Structures Polymers

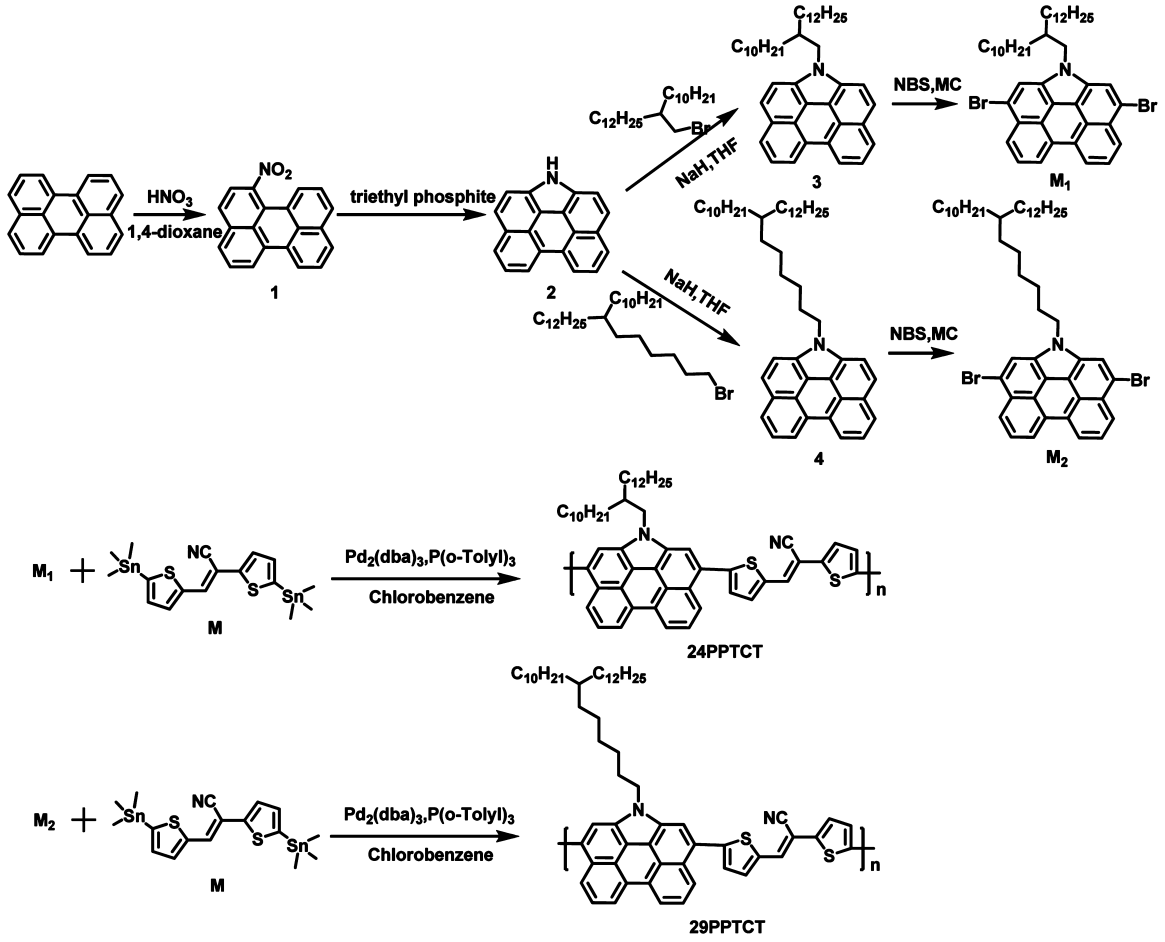

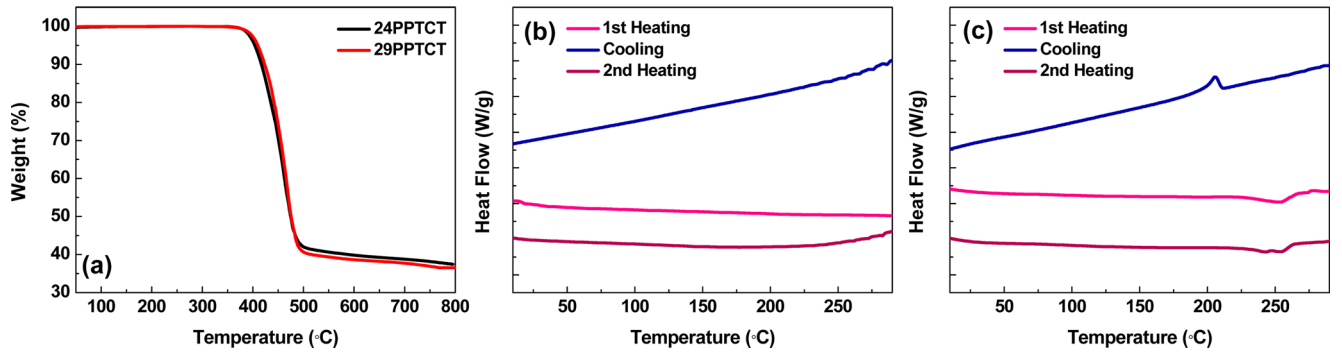

Figure 1. (a) TGA plots of two polymers and DSC graph of (b) 24PPTCT and (c) 29PPTCT with a heating rate of 10 °C/min under a nitrogen atmosphere.

source measurement unit. An Oriel xenon lamp (450 W) with an AM1.5G filter was employed as a solar simulator, with the light intensity calibrated to 100 mW/cm^2 using a silicon cell with a KG5 filter calibrated by the National Renewable Energy Laboratory. EQE spectra were obtained using a photomodulation spectroscopic setup (model Merlin, Oriel), a calibrated Si UV detector, and a SR570 low-noise current amplifier. A hole-only device was fabricated by spin coating PEDOT:PSS (Clevios P VP AI 4083, ca. 40 nm) onto the precleaned ITO, followed by coating with the pure polymer and BHJ film, using the same method as was used to fabricate the solar cells. Finally, a 100 nm thick layer of Au was thermally evaporated onto the active film. All characterization experiments were performed in an ambient atmosphere.

RESULTS AND DISCUSSION

Synthesis and Characterization of Polymers. To investigate the effects of the side chain length on the photovoltaic properties of OSCs, two polymers based on 2-decyltetradecyl and 7-decylnonadecyl-substituted *N*-annulated pyrrolo-perylene were prepared. The backbone structures of these two polymers were identical such that any observed differences in bulk properties could be correlated to differences in side chain structure. The chemical structures and synthetic paths for these materials are shown in Scheme 1. Two alternating copolymers were obtained via typical Stille coupling polymerization at 110 °C and 48 h. To obtain the pure polymer, we subjected the polymer products to successive

DOI: 10.1021/acsami.5b01444
ACS Appl. Mater. Interfaces 2015, 7, 8859−8867

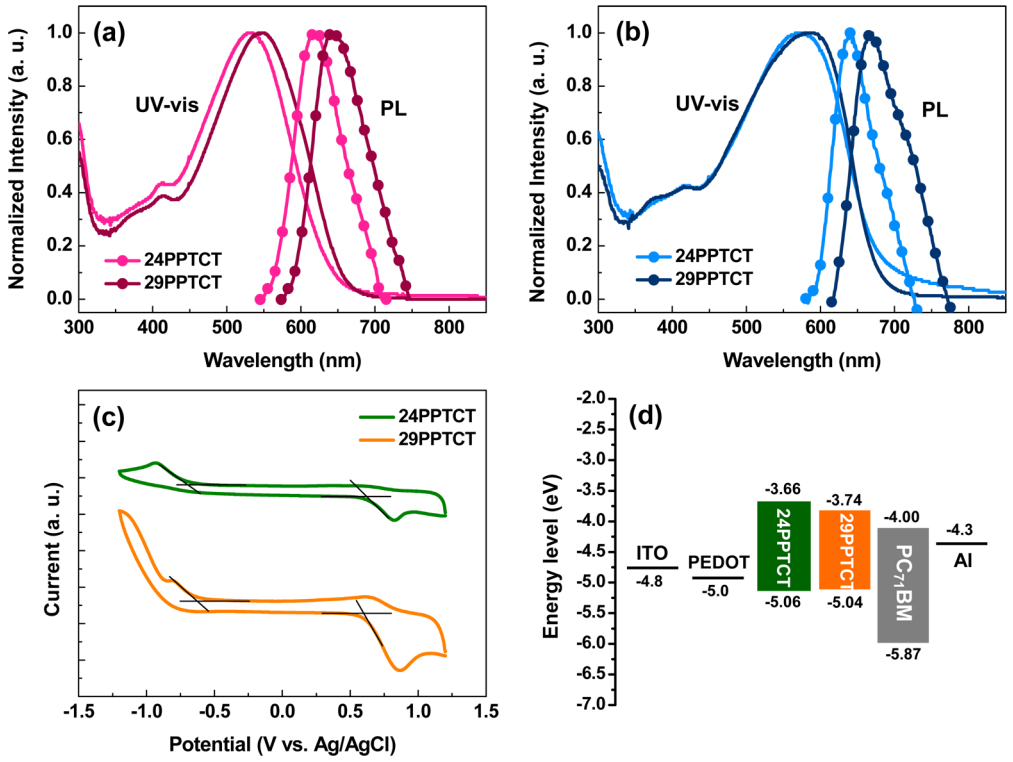

Figure 2. Normalized absorption and PL spectra of two synthesized polymers; in (a) dilute chloroform solutions and (b) films. (c) Cyclic voltammograms of 24PPTCT and 29PPTCT. (d) Energy level diagram of the materials in the conventional photovoltaic device.

Table 1. Optoelectronic Properties of 24PPTCT and 29PPTCT

	UV−vis absorption spectrum				cyclic voltammetry			
polymer	λ_{max} (nm) solution	λ_{max} (nm) film	λ_{onset} (nm) film	E_g^{opt} (eV)[a]	E_{onset}^{ox} (eV)	E_{onset}^{red} (eV)	E_{HOMO} (eV)	E_{LUMO} (eV)
24PPTCT	530	572	701	1.76	0.66	−0.70	−5.06	−3.66
29PPTCT	549	587	715	1.73	0.64	−0.62	−5.04	−3.74

[a]Estimated from the absorption edge in film (E_g^{opt} = 1240/λ_{onset} eV).

Soxhlet extractions with methanol, acetone, hexane, and chloroform. The monomer structures were confirmed by mass spectrometry and NMR spectroscopy. Polymer structures were confirmed by analyses of H NMR spectra. The synthesized polymers were all soluble at room temperature in common halogenated organic solvents (chloroform, chlorobenzene, and 1,2-dichlorobenzene). The molecular weights of the synthesized polymers and their polydispersity indices (PDIs) were estimated by gel permeation chromatography (GPC). The number-average molecular weights (M_n) of 24PPTCT and 29PPTCT were 21 200 and 23 400 g/mol, respectively, with PDIs of 1.42 and 1.31, respectively.

TGA and DSC were used to elucidate the thermal properties of the synthesized polymers. Figure 1a shows thermogravimetric curves of the two copolymers obtained under a nitrogen flow. Both copolymers exhibited high thermal stability, showing less than 5% weight loss during heating to ca. 405 °C, a desirable characteristic for OSC polymers.[23] Interestingly, DSC thermograms (Figures 1b,c) showed no apparent thermal transition for 24PPTCT, implying that this polymer exists in an amorphous state at room temperature.[24] In contrast, 29PPTCT, which contains an linear alkyl spacer (C6), showed distinct melting and crystallization transitions at 253 and 205 °C, respectively. This suggests that the relatively planar structure of 29PPTCT results in a lower degree of steric hindrance and less torsional interactions, which in turn result in stronger intermolecular $\pi-\pi$ interactions.[25]

Optical Properties. Normalized UV−vis absorption spectra of 24PPTCT and 29PPTCT in dilute solutions and in the form of spin-coated films from chloroform are shown in Figures 2a,b. A summary of the absorption data, including absorption maxima and the corresponding band edges, is provided in Table 1. Two absorption bands covering a broad range were observed. Whether in solution or as a thin film, 29PPTCT exhibited red-shifted absorption peaks relative to those of 24PPTCT. This finding is consistent with the DSC analysis, which suggested that the 7-decylnonadecyl chain of 29PPTCT allows the molecule to adopt a more planar structure by the stronger intermolecular interactions.[26]

For both polymers, the absorption spectra in solution were similar to those obtained from thin films, the latter exhibiting clear red-shifts in absorption maxima. Such shifts are generally observed in conjugated systems and are due to aggregation of the polymer main chain and interchain interactions in the solid state.[27] The optical bandgaps calculated from these spectra were 1.76 eV (absorption edge ∼701 nm) for 24PPTCT and 1.73 eV for 29PPTCT (absorption edge ∼715 nm).

Photoluminescence (PL) spectra of two copolymers in chloroform solution and in the thin film state are also shown in Figure 2a,b. 24PPTCT and 29PPTCT are both red emitters,

DOI: 10.1021/acsami.5b01444
ACS Appl. Mater. Interfaces 2015, 7, 8859−8867

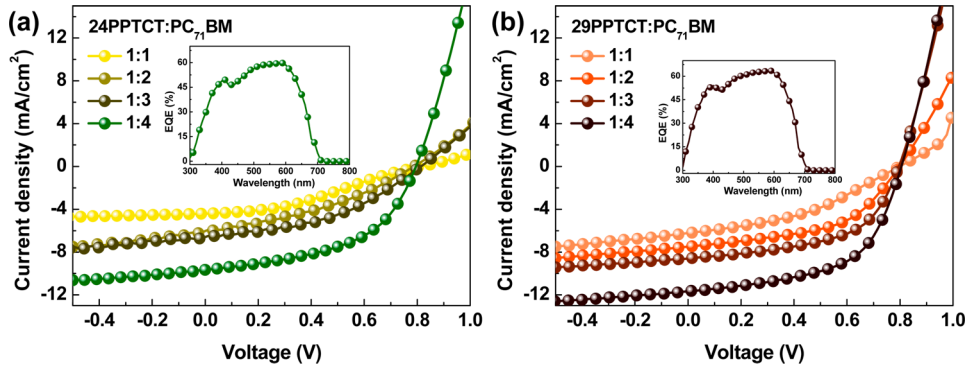

Figure 3. *J*–*V* curves of photovoltaic devices using (a) 24PPTCT and (b) 29PPTCT as active layers.

with solution spectra maxima at 618 and 645 nm, respectively. Compared to the solution spectra, the maximum solid state emission of 24PPTCT was red-shifted to 640 nm, while the 29PPTCT maximum emission showed a red-shift to 669 nm.

Electrochemical Properties. Cyclic voltammetry (CV) was used to characterize the electrochemical behavior and highest occupied molecular orbital (HOMO) and lowest unoccupied molecular orbital (LUMO) energy levels of the synthesized polymers. Electrochemical data are summarized in Table 1. The HOMO/LUMO levels of 24PPTCT and 29PPTCT were calculated from the onset potentials of voltammetric redox peaks relative to oxidation potential of ferrocene, 4.8 eV below the vacuum level, as shown by the following equation.[28,29]

$$\text{HOMO} = -[E_{\text{onset}}^{\text{ox}} - E_{\text{ox}}(\text{ferrocene})] - 4.8\ \text{eV}$$

$$\text{LUMO} = -[E_{\text{onset}}^{\text{red}} - E_{\text{ox}}(\text{ferrocene})] - 4.8\ \text{eV}$$

The calculated HOMO levels of 24PPTCT and 29PPTCT were −5.06 and −5.04 eV, respectively. The calculated LUMO levels were −3.66 eV for 24PPTCT and −3.74 eV for 29PPTCT. Thus, the electrochemically obtained HOMO energy level of 29PPTCT was only slightly higher than that of 24PPTCT, likely due to the effects of the longer 7-decylnonadecyl chain of the side group. These observations, in combination with the UV–vis absorption data, suggest that the backbone of 29PPTCT is more planar than that of 24PPTCT, possibly because the branched alkyl chains exhibit less steric hindrance or due to more extended intermolecular π–π interactions.[30]

Relatively high open-circuit potentials (V_{oc}) should be generated in photovoltaic devices based on these conjugated polymers because V_{oc} is determined primarily by the energy difference between the HOMO of the donor and the LUMO of the acceptor.[31] Also note that these polymers boast ideal LUMO energy levels for effective charge transfer to acceptor materials (Figure 2d).[32] Therefore, both 24PPTCT and 29PPTCT are suitable for further applications in photovoltaic devices.

Photovoltaic Performance. To demonstrate the effect(s) of alkyl chain length on photovoltaic performance, devices comprising a ITO/PEDOT:PSS/copolymers:$PC_{71}BM$/Al structure were fabricated. A solution of polymer and $PC_{71}BM$ in *o*-dichlorobenzene (a total concentration 40 mg/mL) was prepared. *o*-Dichlorobenzene was used because uniform, pinhole-free films tend to form when this solvent is slowly evaporated. The donor/acceptor weight ratio reportedly impacts photovoltaic performance. Therefore, devices based on 24PPTCT or 29PPTCT:$PC_{71}BM$ with different donor/acceptor weight ratios (1:1, 1:2, 1:3, and 1:4) were fabricated. The corresponding *J*–*V* characteristics curves are presented in Figure 3, and the performance parameters of photovoltaic devices are summarized in Table 2. The optimal polymer/

Table 2. Summarized Performance of Devices Containing 24PPTCT and 29PPTCT

polymer: PCBM	blend ratios	V_{oc} (V)	J_{sc} (mA/cm^2)	FF (%)	PCE (%)
24PPTCT:$PC_{71}BM$	1:1	0.81	4.4	35.1	1.32
	1:2	0.79	5.9	36.2	1.71
	1:3	0.81	6.2	42.1	2.11
	1:4	0.80	9.5	47.8	3.63
29PPTCT:$PC_{71}BM$	1:1	0.80	6.2	38.6	2.01
	1:2	0.80	7.5	50.4	3.00
	1:3	0.79	8.6	55.7	3.78
	1:4	0.80	11.3	54.4	4.80

$PC_{71}BM$ ratio in terms of best solar cell performance was 1:4 for both polymers. The 24PPTCT:$PC_{71}BM$ device produced an open circuit voltage (V_{oc}) of 0.80 V, a short-circuit current (J_{sc}) of 9.5 mA cm^{-2}, a fill factor (FF) of 47.8%, and a PCE of 3.63%. The 29PPTCT:$PC_{71}BM$ device showed a PCE of 4.80% with V_{oc} = 0.80 V, J_{sc} = 11.3 mA cm^{-2}, and FF = 54.4%. Higher PCEs were obtained with the 29PPTCT:$PC_{71}BM$ device than with the 24PPTCT:$PC_{71}BM$ cell. This effect was due primarily to the higher J_{sc} and FF values of the latter polymer. Generally, in polymer solar cells, the J_{sc} and FF values are affected by surface morphology and hole mobility as discussed below.

To further improve the photovoltaic performance of the pyrrolo-perylene-based solar cells, a Ca/Al layer is used to replace the only Al layer, so that the cathode can collect electrons more efficiently. Thus, the PCE is elevated to 4.95%, with a larger J_{sc} of 11.5 mA cm^{-2}, a V_{oc} of 0.81, and a FF of 54.6% for the 29PPTCT:$PC_{71}BM$ device. This efficiency of 4.95% achieved by 29PPTCT-based device is higher than those from most reported pyrrolo-perylene-based donors. Under the same deivce conditions, the PCE of the 24PPTCT:$PC_{71}BM$ device is 4.26% (J_{sc} = 10.7 mA cm^{-2}, V_{oc} = 0.81 V, and FF = 49.2%).

To understand why the 29PPTCT:$PC_{71}M$-based device exhibited high PCE values, EQE curves were generated under optimized conditions. As depicted in the insets of Figure 3, both copolymers exhibited efficient photoresponses from 300 to 700 nm, corresponding to a maximum EQE of 63% for the 29PPTCT:$PC_{71}BM$ device and 58% for the

DOI: 10.1021/acsami.5b01444
ACS Appl. Mater. Interfaces 2015, 7, 8859–8867

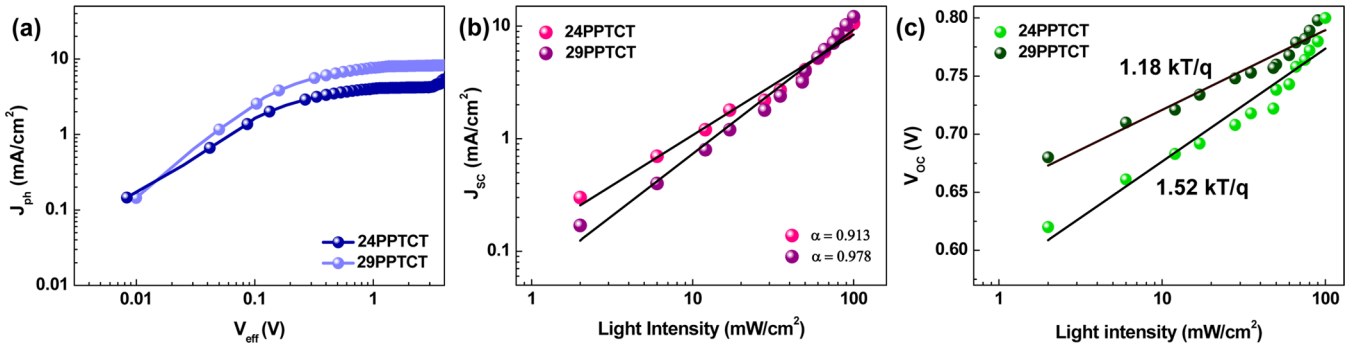

Figure 4. (a) Photocurrent density (J_{ph}) plotted against the effective applied voltage (V_{eff}) for the 24PPTCT and 29PPTCT devices. (b) Light intensity dependence of J_{sc} on a logarithmic scale. Fitting a power law to these data yields α. (c) Measured V_{oc} of photovoltaic cells processed with 24PPTCT and 29PPTCT as a function of illumination intensity, together with linear fits to the data.

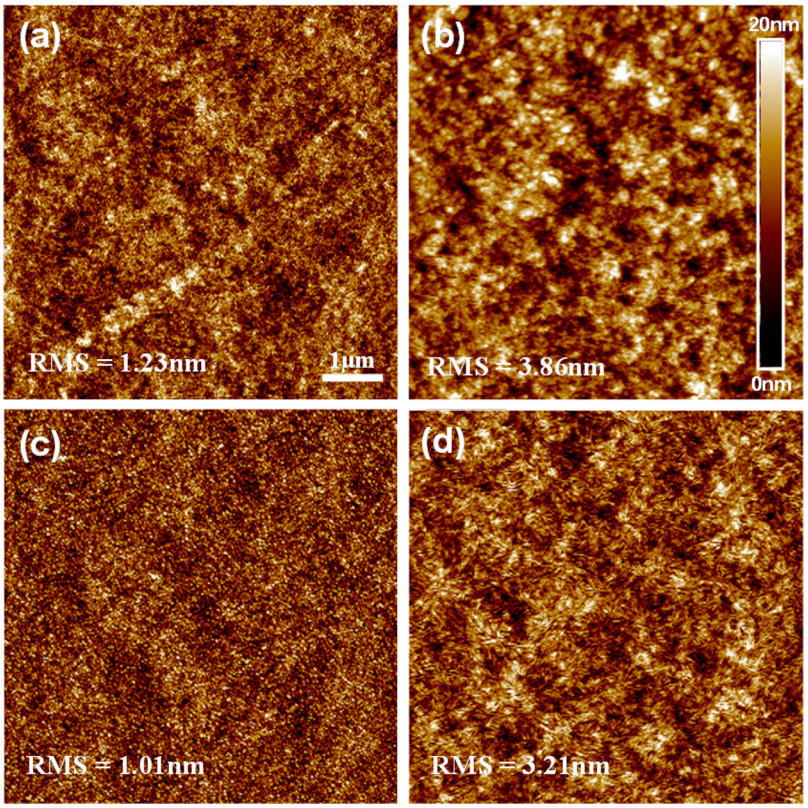

Figure 5. AFM images of (a and b) polymer-only films and (c and d) 24PPTCT or 29PPTCT:$PC_{71}BM$ blend films (1:4 w/w).

24PPTCT:$PC_{71}BM$ device. Higher EQE values are responsible for the higher J_{sc} values of the 29PPTCT-based polymer solar cells.[33] According to the EQE curves and the solar irradiation spectrum, the integral J_{sc} values of the 24PPTCT- and 29PPTCT-based OSCs are 8.9 mA cm^{-2} and 10.7 mA cm^{-2}, respectively, which agree with measured J_{sc} values within a 5% error.

Effects of Recombination on Efficiency. Figure 4a shows the experimental photocurrent as a function of an effective applied voltage (V_{eff}) under two different conditions. The photocurrent (J_{ph}) was calculated as $J_{ph} = J_L - J_D$, where J_L and J_D are the current density under illumination and in the dark, respectively. V_{eff} is defined as $V_{eff} = V_0 - V$, where V_0 is the voltage at which J_{ph} is zero and V is the applied voltage. For $V_0 - V > 0.1$ V, the photocurrent was dependent on the square root of the voltage due to charge recombination effects, as described by the equation

$$J_{ph} = qG\sqrt{\mu_{h(e)}\tau_{h(e)}}\sqrt{V}$$

Here, G is the free charge carrier generation rate, $\mu_{h(e)}$ and $\tau_{h(e)}$ are the mobility and lifetime, each carrier, respectively.[34,35] As shown in Figure 4a, the 29PPTCT photocurrent of within the square root regime ($V_0 - V > 0.1$) was higher than that of the 24PPTCT copolymer. This suggests a lower rate of charge recombination in the 29PPTCT because of intermolecular interactions and the effect(s) of the C6 alkyl spacer, which suppress recombination reactions and increase both J_{sc} and FF.[36]

To obtain further information on the charge recombination kinetics, the variation in J_{sc} with changes in illumination intensity was examined (Figure 4b; data are plotted on a log–log scale and fitted to a power law). J_{sc} can be correlated to illumination intensity (I) by

DOI: 10.1021/acsami.5b01444
ACS Appl. Mater. Interfaces 2015, 7, 8859–8867

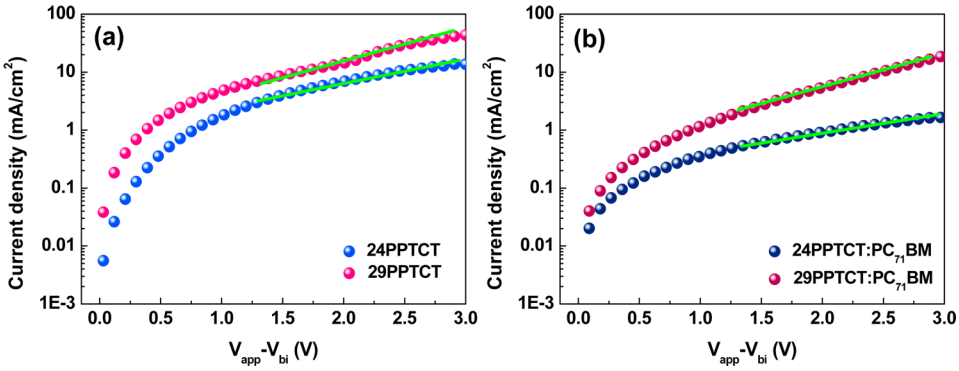

Figure 6. Dark $J-V$ characteristics of hole-only device for (a) pure polymers and (b) polymer:$PC_{71}BM$ blends.

$$J_{sc} \propto I^{\alpha}$$

At short circuit, minimal bimolecular recombination ($\alpha \sim 1$) is required to achieve the highest carrier sweep out, with deviations from $\alpha \sim 1$ indicating the presence of bimolecular recombination.[37] A fit of the data in Figure 4b yielded exponential factors (α) of 0.913 and 0.978 for devices processed with 24PPTCT and 29PPTCT, respectively, under optimal conditions. The α of 24PPTCT is relatively far from unity, indicating that bimolecular recombination is substantial in this device. However, α increases to 0.978 for devices processed with the 29PPTCT polymer. The almost linear dependence of J_{sc} indicates that sweep-out at short circuit is very efficient, while bimolecular recombination is relatively weak. These results suggest that the lower rate of bimolecular recombination results in relatively high J_{sc} and FF values in the 29PPTCT device, thereby resulting in enhanced device performance.[38,39]

Recombination mechanisms were also extracted from curves of V_{oc} as a function of light intensity, as shown in Figure 4c. The photocurrent at V_{oc} is zero; hence all recombination of photogenerated carriers occurs within the cell. Thus, by studying recombination at V_{oc}, valuable information can be extracted regarding various mechanisms. V_{oc} and light intensity (I) are related as follows:

$$V_{oc} \cong \frac{1}{e}(E_{LUMO} - E_{HOMO} - \Delta) - \frac{kT}{e}In(I)$$

where e is the elementary charge, k is the Boltzmann constant, T is temperature in Kelvin, and Δ represents the relatively small band tailing to energy below the acceptor LUMO. Thus, for bimolecular recombination

$$V_{oc} \cong \frac{kT}{e}\mathrm{In}(I) + C(\mathrm{constant})$$

Under this expression, the slope of a plot V_{oc} against $\mathrm{In}(I)$ will be kT/e for bimolecular recombination. Monomolecular recombination, by contrast, shows a stronger dependence, with a slope of $2kT/e$.[40−42] The slope of the curve in Figure 4b corresponding to the device made with 29PPTCT is 1.18 kT/e, implying that only bimolecular recombination occurs at open circuit. In contrast, the analogous slope for the 24PPTCT device is 1.52 kT/e, indicating that both monomolecular and bimolecular recombination occur in this device.

Film Morphology. Atomic force microscopy (AFM) in tapping mode was used to examine the surface morphologies of the active layers of the OSCs. Figure 5 shows the topographic images of the pure and blend films processed with two different polymers. To ensure accurate comparisons, the blend films were prepared under conditions equivalent to those used when fabricating the pure polymer devices.

The 24PPTCT film (Figure 5a) exhibits a flat, relatively formless with a root-means-squared (RMS) roughness of 1.23 nm. However, the spin-coated film from pure 29PPTCT (Figure 5b) shows clearly aggregated domains and increased phase separation with a larger RMS roughness of 3.86 nm. Moreover, in the 24PPTCT-blend film (Figure 5c), no obvious evidence of phase separation of 24PPTCT and $PC_{71}BM$ is observed, indicating homogeneous mixing of the components. The surface processed with 24PPTCT and $PC_{71}BM$ is also very smooth, with RMS surface roughness of 1.01 nm. When 29PPTCT, which contains a linear alkyl spacer (C6), was used in the blend rather than 24PPTCT, the film morphology changed markedly (29PPTCT:$PC_{71}BM$; Figure 5d). Aggregated structures with randomly oriented domains 25−50 nm wide are observed, and the film becomes rougher (RMS roughness 3.21 nm). The aggregated domains probably originate from the enhanced intermolecular interactions in 29PPTCT.[43] The increased surface roughness also indicates an increase in the self-organized ordering of the polymer.[44] The higher surface roughness and ordering of the crystalline domain in the 29PPTCT system are expected to provide separate pathways for electrons and holes, and to increase J_{sc} in the 29PPTCT system.[45]

Charge Transport. In BHJ solar cells, photogenerated charge extraction at the electrode decreases with increasing carrier sweep-out, which is limited by carrier mobility and loss of photogenerated carriers by recombination; hence, the mobility of charge carriers in the active film is a critical factor. We therefore examined the hole mobility in pure polymer and polymer:$PC_{71}BM$ films by measuring the dark current density−voltage ($J-V$) behavior. The $J-V$ data were analyzed using a space-charge limited current (SCLC) model described by the Mott−Gurney law, which includes a small field-dependent term as shown in the following equation:

$$J = \frac{9}{8}\varepsilon_0\varepsilon_r\mu_h\frac{(V_{appl} - V_r - V_{bi})^2}{L^3}\exp\left(\beta\sqrt{\frac{V_{appl} - V_r - V_{bi}}{L}}\right)$$

where J represents the current density, L is the film thickness of the active layer, μ_h is hole mobility, $\varepsilon_0\varepsilon_r$ represents the dielectric permittivity of the active layer, V_{appl} is the applied voltage, V_r represents the voltage drop due to contact resistance and series resistance across the electrodes, V_{bi} is built-in voltage, and β is the field activation factor.[46]

DOI: 10.1021/acsami.5b01444
ACS Appl. Mater. Interfaces 2015, 7, 8859−8867

Figure 6 shows experimental $J-V$ curves from the hole-only device ITO/PEDOT:PSS/polymer or polymer:$PC_{71}BM$/Au. Fitting to the experimental results revealed hole mobilities in pure polymer films of 1.62×10^{-4} cm^2 V^{-1} s^{-1} for 24PPTCT and 4.31×10^{-4} cm^2 V^{-1} s^{-1} for 29PPTCT. The observed increase in hole mobility in the 29PPTCT polymer agrees well with morphological analyses, which showed higher degrees of domain aggregation and crystallinity when 29PPTCT was used to the donor material.[47]

Figure 6b shows that hole mobilities of the polymer:$PC_{71}M$ blend films were similar to those of pure polymer films. Higher hole mobilities were also observed in blends of 29PPTCT and $PC_{71}BM$ (1.22×10^{-4} cm^2 V^{-1} s^{-1}), relative to those in blends of 24PPTCT:$PC_{71}BM$ (8.79×10^{-5} cm^2 V^{-1} s^{-1}). These results indicate that stronger intermolecular interactions in 29PPTCT resulted in higher hole mobilities in the BHJ films and enhanced the stability of charge−exciton separation, both of which improved the charge transport properties of the hole carrier.[48]

CONCLUSION

We systematically investigated the effect of the geometry of alkyl side chains on the optoelectronic and photovoltaic properties of pyrrolo-perylene-based polymers. We found that, when 2-decyltetradecyl side chains were replaced with 7-decylnonadecyl side-chains, both the electronic properties and film morphology changed markedly. 29PPTCT, which contains 7-decylnonadecyl side chains, exhibited more red-shifted light absorption, a smaller band gap, a more planar structure, and a higher hole mobility than 24PPCT, which contains 2-decyltetradecyl side chains. The introduction of 7-decylnonadecyl side-chains increased the J_{sc} and FF values of polymer solar cells made with these materials. The 29PPTCT devices exhibited the best overall performance of 4.80% PCE with a V_{oc} of 0.80 V, a J_{sc} of 11.3 mA cm^{-2}, and a FF of 54.4%. Intensity-dependent $J-V$ curves revealed that bimolecular recombination was suppressed in 29PPTCT devices. In addition, the dominance of bimolecular recombination when approaching open circuit and the lack of monomolecular recombination at open circuit resulted in high J_{sc} and FF values.

AUTHOR INFORMATION

Corresponding Authors

*E-mail: ykim@gnu.ac.kr

*E-mail: cep@postech.ac.kr.

Author Contributions

[‖]These authors contributed equally to this work.

Notes

The authors declare no competing financial interest.

ACKNOWLEDGMENTS

This study was supported by a grant (2011-0031639) from the Center for Advanced Soft Electronics under the Global Frontier Research Program of the Ministry of Education, Science and Technology. This work was also supported by the National Research Foundation of Korea Grant funded by the Korean Government (MSIP; 2010-0029084 and 2012M3A7B4049647)

REFERENCES

(1) Li, G.; Zhu, R.; Yang, Y. Polymer Solar Cells. *Nat. Photonics* **2012**, *6*, 153−161.

(2) Cheng, Y.-J.; Yang, S.-H.; Hsu, C.-S. Synthesis of Conjugated Polymers for Organic Solar Cell Applications. *Chem. Rev.* **2009**, *109*, 5868−5923.

(3) Beaujuge, P. M.; Frechet, J. M. J. Molecular Design and Ordering Effects in π-Functional Materials for Transistor and Solar Cell Applications. *J. Am. Chem. Soc.* **2011**, *133*, 20009−20029.

(4) Zheng, Z.; Zhang, S.; Zhang, M.; Zhao, K.; Ye, L.; Chen, Y.; Yang, B.; Hou, Z. Highly Efficient Tandem Polymer Solar Cells with a Photovoltaic Response in the Visible Light Range. *Adv. Mater.* **2015**, *27*, 1189−1194.

(5) Ye, L.; Zhang, S.; Zhao, W.; Yao, H.; Hou, J. Highly Efficient 2D-Conjugated Benzodithiophene-Based Photovoltaic Polymer with Linear Alkylthio Side Chain. *Chem. Mater.* **2014**, *26*, 3603−3605.

(6) Zhang, L.; Cao, Y.; Colella, N. S.; Liang, Y.; Bredas, J.-L.; Houk, K. N.; Briseno, A. L. Unconventional, Chemically Stable, and Soluble Two-Dimensional Angular Polycyclic Aromatic Hydrocarbons: From Molecular Design to Device Applications. *Acc. Chem. Res.* **2015**, *48*, 500−509.

(7) Jackson, N. E.; Savoie, B. M.; Kohlstedt, K. L.; Marks, T. J.; Chen, L. X.; Ratner, M. A. Structural and Conformational Dispersion in the Rational Design of Conjugated Polymers. *Macromolecules* **2014**, *47*, 987−992.

(8) Li, Y.; Zhang, Z.-G. Side-Chain Engineering of High-Efficiency Conjugated Polymer Photovoltaic Materials. *Sci. China Chem.* **2015**, *58*, 192−209.

(9) Kesters, J.; Verstappen, P.; Raymakers, J.; Vanomelingen, W.; Drijkoningen, J.; D'Haen, J.; Manca, J.; Lutsen, L.; Vanderzande, D.; Maes, W. Enhanced Organic Solar Cell Stability by Polymer (PCPDTBT) Side Chain Functionalization. *Chem. Mater.* **2015**, *27*, 1332−1341.

(10) Warnan, J.; Cabanetos, C.; Labban, A. E.; Hansen, M. R.; Tassone, C.; Toney, M. F.; Beaujuge, P. M. Ordering Effects in Benzo[1,2-*b*:4,5-*b*′]difuran-thieno[3,4-*c*] pyrrole-4,6-dione Polymers with >7% Solar Cell Efficiency. *Adv. Mater.* **2014**, *26*, 4357−4362.

(11) Li, Y. Molecular Design of Photovoltaic Materials for Polymer Solar Cells: Toward Suitable Electronic Energy Levels and Broad Absorption. *Acc. Chem. Res.* **2014**, *45*, 723−733.

(12) Lee, J.; Han, A.-R.; Yu, H.; Shin, T. J.; Yang, C.; Oh, J. H. Boosting the Ambipolar Performance of Solution-Processable Polymer Semiconductors via Hybrid Side-Chain Engineering. *J. Am. Chem. Soc.* **2013**, *135*, 9540−9547.

(13) Wu, J.-S.; Cheng, S.-W.; Cheng, Y.-J.; Hsu, C.-S. Donor-Acceptor Conjugated Polymers Based on Multifused Ladder-Type Arenes for Organic Solar Cells. *Chem. Soc. Rev.* **2015**, *44*, 1113−1154.

(14) Dang, D.; Chen, W.; Himmelberger, S.; Tao, Q.; Lundin, A.; Yang, R.; Zhu, W.; Salleo, A.; Muller, C.; Wang, E. Enhanced Photovoltaic Performance of Indacenodithiohene-Quinoxaline Co-polymers by Side-Chain Modulation. *Adv. Energy Mater.* **2014**, *4*, 1400680.

(15) Zhang, S.; Ye, L.; Zhao, W.; Liu, D.; Yao, H.; Hou, J. Side Chain Selection for Designing Highly Efficient Photovoltaic Polymers with 2D-Conjugated Structure. *Macromolecules* **2014**, *47*, 4653−4659.

(16) Xu, X.; Wu, Y.; Fang, J.; Li, Z.; Wang, Z.; Li, Y.; Peng, Q. Side-Chain Engineering of Benzodithiophene-Fluorinated Quinoxaline Low-Band-Gap Co-polymers for High-Performance Polymer Solar Cells. *Chem.—Eur. J.* **2014**, *20*, 13259−13271.

(17) Wan, M.; Wu, W.; Sang, G.; Zou, Y.; Liu, Y.; Li, Y. Poly(thienylvinylene-thienylene) with Cyano Substituent: Synthesis and Application in Field-Effect Transistor and Polymer Solar Cell. *J. Polym. Sci., Part A: Polym. Chem.* **2009**, *47*, 4028−4036.

(18) Cha, H.; Kim, H. N.; An, T. K.; Kang, M. S.; Kwon, S.-K.; Kim, Y.-H.; Park, C. E. Effects of Cyano-Substituents on the Molecular Packing Structures of Conjugated Polymers for Bulk-Heterojunction Solar Cells. *ACS. Appl. Mater. Interfaces* **2014**, *6*, 15774−15782.

(19) Chen, H.; He, C.; Yu, G.; Zhao, Y.; Huang, J.; Zhu, M.; Liu, H.; Guo, Y.; Li, Y.; Liu, Y. Phenanthro[1,10,9,8-*cdefg*]carbazole-Containing Copolymer for High Performance Thin-Film Transistors and Polymer Solar Cells. *J. Mater. Chem.* **2012**, *22*, 3696−3698.

DOI: 10.1021/acsami.5b01444
ACS Appl. Mater. Interfaces 2015, 7, 8859−8867

(20) Park, K. H.; Yun, H.-J.; Lu, W.; Chung, D. S.; Kwon, S.-K.; Kim, Y.-H. A New Class of Organic Semiconductors for Solution processed OTFTs: Synthesis and Characterization of Pyrrolo-Perylene Derivatives with Different End Groups. *Dyes Pigments* **2014**, *103*, 214−221.
(21) Park, S. M.; Yoon, Y.; Jeon, C. W.; Kim, H.; Ko, M. J.; Lee, D. K.; Kim, J. Y.; Son, H. J.; Kwon, S. K.; Kim, Y. H.; Kim, B. S. Synthesis of Phenanthro[1,10,9,8-cdefg]carbazole-based Conjugated Polymers for Organic Solar Cell Applications. *J. Polym. Sci., Part A: Polym. Chem.* **2014**, *52*, 796−803.
(22) Yun, H.-J.; Kang, S.-J.; Yong, X.; Kim, S. O.; Kim, Y.-H.; Noh, Y.-Y.; Kwon, S.-K. Dramatic Inversion of Charge Polarity in Diketopyrrolopyrrole-Based Organic Field-Effect Transistors via a Simple Nitrile Group Substitution. *Adv. Mater.* **2014**, *26*, 7300−7307.
(23) Deng, Y.; Liu, J.; Wang, J.; Liu, L.; Li, W.; Tian, H.; Zhang, X.; Xie, Z.; Geng, Y.; Wang, F. Dithienocarbazole and Isoindigo based Amorphous Low Bandgap Conjugated Polymers for Efficient Polymer Solar Cells. *Adv. Mater.* **2014**, *26*, 471−476.
(24) Kim, Y. J.; Cheon, Y. R.; Jang, J.-W.; Kim, Y.-H.; Park, C. E. A Potential Naphtho[2,1-*b*:3,4-*b*′]dithiophene-based Polymer with Large Open Circuit Voltage for Efficient use in Organic Solar Cells. *J. Mater. Chem. C* **2015**, *3*, 1904−1912.
(25) Eisenmenger, N. D.; Su, G. M.; Welch, G. C.; Takacs, C. J.; Bazan, G. C.; Kramer, E. J.; Chabinyc, M. L. Effect of Bridging Atom Identity on the Morphological Behavior of Solution-Processed Small Molecule Bulk Heterojunction Photovoltaics. *Chem. Mater.* **2013**, *25*, 1688−1698.
(26) Gao, J.; Dou, L.; Chen, W.; Chen, C.-C.; Guo, X.; You, J.; Bob, B.; Chang, W.-H.; Strzalka, J.; Wang, C.; Li, G.; Yang, Y. Improving Structural Order for a High-Performance Diketopyrrolopyrrole-Based Polymer Solar Cell with a Thick Active layer. *Adv. Energy Mater.* **2014**, *4*, 1300739.
(27) Wang, D. H.; Pron, A.; Leclerc, M.; Heeger, A. J. Additive-Free Bulk-Heterojuction Solar Cells with Enhanced Power Conversion Efficiency, Comprising a Newly Designed Selenophene-Thienopyrrolodione Copolymer. *Adv. Funct. Mater.* **2013**, *23*, 1297−1304.
(28) Dong, Y.; Hu, X.; Duan, C.; Liu, P.; Liu, S.; Lan, L.; Chen, D.; Ying, L.; Su, S.; Gong, X.; Huang, F.; Cao, Y. A Series of New Medium-Bandgap Conjugated Polymers Based on Naphtho[1,2-*c*:5,6-*c*]bis(2-octyl-[1,2,3]triazole) for High-Performance Polymer Solar Cells. *Adv. Mater.* **2013**, *25*, 3683−3688.
(29) Cheon, Y. R.; Kim, Y. J.; Ha, J.-j.; Kim, M.-J.; Park, C. E.; Kim, Y.-H. TPD-Based Copolymers with Strong Interchain Aggregation and High Hole Mobility for Efficient Bulk Heterojunction Solar Cells. *Macromolecules* **2014**, *47*, 8570−8577.
(30) Kang, I.; Yun, H.-J.; Chung, D. S.; Kwon, S.-K.; Kim, Y.-H. Record High Hole Mobility in Polymer Semiconductors via Side-Chain Engineering. *J. Am. Chem. Soc.* **2013**, *135*, 14896−14899.
(31) Zhou, P.; Zhang, Z.-G.; Li, Y.; Chen, X.; Qin, J. Thiophene-Fused Benzothiadiazole: A Strong Electron-Acceptor Unit to Build D−A Copolymer for Highly Efficient Polymer Solar Cells. *Chem. Mater.* **2014**, *26*, 3495−3501.
(32) Jo, J.; Pron, A.; Berrouard, P.; Leong, W. L.; Yuen, J. D.; Moon, J. S.; Leclerc, M.; Heeger, A. J. A New Terhiophene-Thienopyrrolodione Copolymer-Based Bulk Heterojunction Solar Cell with High Open-Circuit Voltage. *Adv. Energy Mater.* **2012**, *2*, 1397−1403.
(33) Intemann, J. J.; Yao, K.; Li, Y.-X.; Yip, H.-L.; Xu, Y.-X.; Liang, P.-W.; Chueh, C.-C.; Ding, F.-Z.; Yang, X.; Li, X.; Chen, Y.; Jen, A. K.-Y. Highly Efficient Inverted Organic Solar Cells Through Material and Interfacial Engineering of Indacenodithieno[3,2-*b*]thiophene-Based Polymers and Devices. *Adv. Funct. Mater.* **2014**, *24*, 1465−1473.
(34) He, Z.; Zhong, C.; Huang, X.; Wong, W.-Y.; Wu, H.; Chen, L.; Su, S.; Cao, Y. Simultaneous Enhancement of Open-Circuit Voltage, Short-Circuit Current Density, and Fill Factor in Polymer Solar Cells. *Adv. Mater.* **2011**, *23*, 4636−4643.
(35) Lee, G.-Y.; Moon, B.-J.; Song, S.; Lee, W. H.; Woo, H. Y.; Park, T. Suppressing Charge Recombination by Incorporating 3,6-Carbazole into Poly[9-(heptadecan-9-yl)-9*H*-carbazole-2,7-diyl-alt-(5,6-bis-(octyloxy)-4,7-di(thiophen-2-yl)benzo[1,2,5]-thiadiazole)-5,5-diyl]. *J. Polym. Sci., Part A: Polym. Chem.* **2014**, *52*, 2047−2056.
(36) Kyaw, A. K. K.; Wang, D. H.; Wynands, D.; Zhang, J.; Nguyen, T.-Q.; Bazan, G. C.; Heeger, A. J. Improved Light Harvesting and Improved Efficiency by Insertion of an Optical Spacer (ZnO) in Solution-Processed Small-Molecule Solar Cells. *Nano Lett.* **2013**, *13*, 3796−3801.
(37) Kyaw, A. K. K.; Wang, D. H.; Luo, C.; Cao, Y.; Nguyen, T.-Q.; Bazan, G. C.; Heeger, A. J. Effects of Solvent Additives on Morphology, Charge Generation, Transport, and Recombination in Solution-Processed Small-Molecule Solar Cells. *Adv. Energy Mater.* **2014**, *4*, 1301469.
(38) Wang, D. H.; Kyaw, A. K. K. Roles of Solvent Additive in Organic Photovoltaic Cells through Intensity Dependence of Current−Voltage Characteristics and Charge Recombination. *Appl. Phys. Lett.* **2014**, *105*, 103301.
(39) Liu, C.; Hu, X.; Zhong, C.; Huang, M.; Wang, K.; Zhang, Z.; Gong, X.; Cao, Y.; Heeger, A. J. The Influence of Binary Processing Additives on the Performance of Polymer Solar Cells. *Nanoscale* **2014**, *6*, 14297−14304.
(40) Zhang, Y.; Dang, X.-D.; Kuik, M.; Cowan, S. R.; Zalar, P.; Kim, C.; Nguyen, T.-Q. High Light Intensity Effects on Nanoscale Open-Circuit Voltage for Three Common Donor Materials in Bulk Heterojunction Solar Cells. *Energy Environ. Sci.* **2013**, *6*, 1766−1771.
(41) Choi, H.; Kim, H.-B.; Ko, S.-J.; Kim, J. Y.; Heeger, A. J. An Organic Surface Modifier to Produce a High Work Function Transparent Electrode for High Performance Polymer Solar Cells. *Adv. Mater.* **2015**, 892−896.
(42) Janssen, R. A. J.; Nelson, J. Factors Limiting Device Efficiency in Organic Photovoltaics. *Adv. Mater.* **2013**, *25*, 1847−1858.
(43) Huang, Y.; Kramer, E. J.; Heeger, A. J.; Bazan, G. C. Bulk Heterojunction Solar Cells: Morphology and Performance Relationships. *Chem. Rev.* **2014**, *114*, 7006−7043.
(44) Bartelt, J. A.; Douglas, J. D.; Mateker, W. R.; Labban, A. E.; Tassone, C. J.; Toney, M. F.; Frechet, J. M. J.; Beaujuge, P. M.; McGehee, M. D. Controlling Solution-Phase Polymer Aggregation with Molecular Weight and Solvent Additives to Optimize Polymer-Fullerene Bulk Heterojunction Solar Cells. *Adv. Energy Mater.* **2014**, *4*, 1301733.
(45) Liu, Y.; Zhao, J.; Li, Z.; Mu, C.; Ma, W.; Hu, H.; Jiang, K.; Lin, H.; Ade, H.; Yan, H. Aggregation and Morphology Control Enables Multiple Cases of High-Efficiency Polymer Solar Cells. *Nat. Commun.* **2014**, *5*, 5293.
(46) Wang, D. H.; Morin, P.-O.; Lee, C.-L.; Kyaw, A. K. K.; Leclerc, M.; Heeger, A. J. Effect of Processing Additive on Morphology and Charge Extraction in Bulk-Heterojunction Solar Cells. *J. Mater. Chem. A* **2014**, *2*, 15052−15057.
(47) Keshtov, M. L.; Marochkin, D. V.; Kochurov, V. S.; Khokhlov, A. R.; Koukaras, E. N.; Sharma, G. D. New Conjugated Alternating Benzodithiophene-Containing Copolymers with Different Acceptor Units: Synthesis and Photovoltaic Application. *J. Mater. Chem. A* **2014**, *2*, 155−171.
(48) Nuzzo, D. D.; Reenen, S.; Janssen, R. A. J.; Kemerink, M.; Meskers, S. C. J. Evidence for Space-Charge-Limited Conduction in Organic Photovoltaic Cells at Open-Circuit Conditions. *Phys. Rev. B* **2013**, *87*, 085207.

DOI: 10.1021/acsami.5b01444
ACS Appl. Mater. Interfaces 2015, 7, 8859−8867